RSC Advances

ROYAL SOCIETY OF CHEMISTRY

www.rsc.org/advances

An efficient method for the synthesis of nickel phosphide nanocrystals *via* thermal decomposition of single-source precursors

Yuan Pan, Yunqi Liu, Chenguang Liu**

State Key Laboratory of Heavy Oil Processing, Key Laboratory of Catalysis, China National Petroleum Corporation (CNPC), China University of Petroleum, 66 West Changjiang Road, Qingdao, Shandong 266580, People's Republic of China

* Corresponding author. E-mail address: liuyq@upc.edu.cn; cgliu1962@sina.com.

Tel.: +86-532-86981861; +86-532-86981716.

Abstract

An efficient method was developed for the synthesis of nickel phosphide nanocrystals (NCs) *via* thermal decomposition of bis(triphenylphosphine)nickel dichloride (BTND) precursor in the presence of oleylamine (OAm) for the first time. The effect of synthetic conditions such as reaction temperature, reaction time and OAm quantity on the size and phase of the as-synthesized nickel phosphide NCs were discussed. The structure and morphology were characterized by X-ray diffraction (XRD), transmission electron microscope (TEM), X-ray photoelectron spectroscopy (XPS) and N_2 adsorption-desorption measurement. The results showed that the size of Ni_2P NCs can be controlled by increasing reaction temperature and OAm quantity. The phase of nickel phosphide NCs can be controlled by changing reaction time. The shorter reaction time was beneficial for forming $Ni_{12}P_5$ NCs, and longer reaction time was beneficial for forming Ni_2P NCs. Furthermore, a possible growth mechanism of the as-synthesized nickel phosphide NCs was proposed. These synthetic techniques may be expanded to other metal phosphide materials.

Keywords: Nickel phosphide nanocrystals; Controlled synthesis; Growth mechanism

1. Introduction

In recent years, increasing attention has been paid to the nanostructured transition metal phosphides because of their excellent physicochemical properties and comprehensive applications in many fields, such as magnetism, photonics and catalysis.[1-3] Among them, nickel phosphide nanocrystals (NCs) are considered to be a new class of highly active catalysts for many reactions, such as hydrodesulfurization

(HDS), hydrodenitrogenation (HDN), photocatalytic degradation and electrocatalytic hydrogen evolution reaction (HER).[4-7] Many studies suggested that the size, phase and shape of nickel phosphide NCs played an important role in the properties.[8] Therefore, it is very interesting to investigate the size-, phase- and shape-dependent catalytic properties of nickel phosphide NCs.

Nowadays, various methods have been attempted to synthesize nickel phosphide NCs, such as thermal decomposition of organometallic precursor,[9-11] solvothermal synthesis,[12-14] the reduction of phosphates[15] and phosphinates,[16] and microwave synthesis.[17] However, these methods are complicated, and it is difficult to realize the control synthesis of nickel phosphide NCs. Generally, the thermal decomposition of organometallic precursor was used due to the reaction can easy to be achieved. For example, Muthuswamy et al. synthesized the $Ni_{12}P_5$ and Ni_2P nanoparticles (NPs) with hollow and solid morphologies by changing synthetic conditions, such as P:Ni precursor ratio, temperature, time and oleylamine (OAm) quantity.[18] Singh et al. synthesized Ni_2P nanorods with different size by changing the number of injections of precursor and reaction time.[19] However, nickel(II) acetylacetonate and trioctylphosphine (TOP) were used as nickel source and phosphorus source to synthesize nickel phosphide NCs in these method. The high price and instability of TOP limited their application.[20] Therefore, new nickel source and phosphorus source need to be developed. Bis(triphenylphosphine)nickel dichloride precursor (BTND), which is an alternative choice for precursor due to the nickel source and phosphorus source are coexist in a compound, which further simplified the reaction process. More

importantly, the size and phase of nickel phosphide NCs also can be controlled by changing reaction conditions.

In this work, an efficient method was developed to synthesize nickel phosphide NCs by one-pot thermal decomposition of bis(triphenylphosphine)nickel dichloride precursor in the presence of OAm for the first time. The effect of synthetic conditions such as reaction temperature, reaction time and OAm quantity on the phase and size of the nickel phosphide NCs were discussed. In addition, a possible growth mechanism of the as-synthesized nickel phosphide NCs was proposed.

2. Experimental

2.1. Materials

Nickel(II) chloride hexahydrate ($NiCl_2 \cdot 6H_2O$, ≥98.0%), triphenylphosphine (PPh_3), hexane (≥99.5%) and ethanol (≥99.7%) were obtained from Sinopharm Chemical Reagent Co., Ltd. Oleylamine (OAm, 95%) was obtained from Aladdin Chemistry Co. Ltd. All chemicals were used as received without further purification. All reactions were carried out under argon atmosphere using standard air-free techniques.

2.2 Synthesis of BTND precursor

The BTND precursor was synthesized using minor modifications of the previously reported method.[21] $NiCl_2 \cdot 6H_2O$ (10 mmol, 2.38 g), PPh_3 (23 mmol, 6.03 g), EtOH (40 mL) were placed in a four-neck flask and stirred magnetically under a flow of argon. The flask was fitted with a reflux condenser, and the mixture was heated to 80 ^oC with a heating rate of 10 $°C \cdot min^{-1}$ and kept at this temperature for one hour. After cooling to room temperature, a dark green solid was obtained from the solution by vacuum

filtration, and then the solid was washed three times with ethanol and ether. Finally, the dark green powder (5.85 g, 89.3 %) was obtained by drying in vacuum at 60 ^{o}C for 24 h.

2.3 Synthesis of nickel phosphide NCs

In a typical reaction, BTND (1 mmol, 0.65 g) and OAm (5 ~ 15 mL) were placed in a four-neck flask and stirred magnetically under a flow of argon. The mixture was raised to 120 ^{o}C at a heating rate of 10 °C·min^{-1} and kept at this temperature for 30 min. Then the mixture was heated to 300 ~ 340 ^{o}C rapidly and maintained for 10 min ~ 5 h. After cooling to room temperature, a black precipitate was obtained from the solution by adding excess ethanol and separated by centrifugation (4000 rpm, 15 min). Then the black precipitate was washed three times with a mixture of hexane and ethanol. Finally, the product was dried in vacuum at 60 ^{o}C for 24 h. The synthetic route is shown in Fig. 1. The size and phase of the as-synthesized nickel phosphide NCs could be controlled by changing synthetic conditions, including reaction temperature, reaction time and OAm quantity.

2.4 Characterization

Elemental analysis was performed on an Elementar Vario ELIII. FT-IR spectrum was collected on a Nexus spectrometer (Nicolet, USA) in the range of 4000~400 cm^{-1} with 32 scans and the samples were prepared as KBr pellets. ^{13}C NMR measurement was carried out on a Bruker DRX 500. ^{13}C chemical shift was reported in parts per million relative to TMS (δ = 0.00 ppm) and was referenced to the residual solvent peak (^{13}C, $CDCl_3$ 77.16 ppm). Combined thermogravimetry and differential scanning

calorimetry (TG-DSC, QMS 403C Aeolos) was carried out at a heating rate of 10 $^{o}C \cdot min^{-1}$ under high-purity nitrogen atmosphere. XRD was performed on a panalytical X'pert PROX-ray diffractometer with Cu Kα monochromatized radiation (λ= 1.54 Å) and operated at 45 kV, 40 mA. TEM was performed on a JEM-2100 UHR microscope (JEOL, Japan) at an accelerating voltage of 200 kV. N_2 adsorption-desorption experiment was carried out on a ChemBET 3000 (Quantachrome, USA) instrument. X-ray photoelectron spectrum (XPS) were performed on a VG ESCALABMK II spectrometer using an Al K_α (1486.6 eV) photon source.

3. Results and discussion

3.1 Characterization of BTND precursor

The C and H elemental contents of the BTND precursor are 66.4 % and 4.12 %, respectively. These values are almost in good agreement with theoretical value (C 66.1 % and H 4.62 %). The FTIR spectrum of the BTND precursor is shown in Fig. 2a. The absorption at 3048 cm^{-1} and 2928 cm^{-1} is due to the stretching vibration of the C-H bond in benzene ring. The absorption response at 1627 cm^{-1}, 1480 cm^{-1} and 1430 cm^{-1} belongs to the stretching vibration of the C=C in benzene ring. The absorption at 1093 cm^{-1} is attributed to the stretching vibration of C-P. The absorption at 745 cm^{-1}, 692 cm^{-1} and 526 cm^{-1} is attributed to the bending vibration of the benzene group. All the absorption peaks are in good agreement with the BTND precursor. The ^{13}C NMR spectrum of the BTND precursor is shown in Fig. 2b. Only four peaks can be observed, which indicate the mono-substitution characteristic of benzene ring. Meanwhile, the chemical shifts at 137.2 ppm, 133.8 ppm, 132.1 ppm and 128.5 ppm are attributed to the C1, C2, C3, and C4 in benzene ring skeleton. Therefore, ^{13}C NMR spectrum coincides with the results of FTIR and elemental analysis and in fair

agreement with the structure of the BTND precursor. The thermal stability of the BTND precursor was studied by TG analysis (Fig. 2c). No initial mass loss around 100 ^{o}C, which indicates that no crystal water or surface absorbed water molecules existed in the BTND precursor. The rapid weight loss of 90% from 195 ^{o}C to 300 ^{o}C is attributed to the decomposition of BTND precursor. In addition, DSC curve shows an endothermic peak at 235 ^{o}C, which indicates that the decomposition of BTND precursor is a strong endothermal reaction.

3.2 Effect of synthetic conditions on size and crystalline phase

In our experiments, the nickel phosphide NCs could be obtained by one-pot thermal decomposition of bis(triphenylphosphine)nickel dichloride precursor in the presence of OAm for the first time. In order to control the size and crystalline phase of the as-synthesized nickel phosphide NCs, three groups of the single-factor experiment were carried out under different conditions, including reaction temperature, reaction time and OAm quantity. Each effect of the three reaction parameters on the size and crystalline phase of the nickel phosphide NCs was studied. The detailed synthetic conditions and the corresponding product for each group are listed in Table 1.

Fig. 3 shows the XRD pattern of the as-synthesized nickel phosphide NCs at different reaction temperature. It can be seen that all the diffraction peaks match well with hexagonal structure of Ni_2P (PDF#03-065-3544), the diffraction peaks at 30.5°, 31.8°, 35.3°, 40.8°, 44.6°, 47.3°, 54.1°, 54.8°, 66.2°, 72.6°, 74.8°, 80.1° and 88.7° are attributed to (110), (101), (200), (111), (201), (210), (300), (211), (310), (311), (400), (401) and (321) crystal faces, and no extraneous peaks exist, which indicates that the as-synthesized Ni_2P is pure phase. Fig. 4a~f show the morphology images and size

distributions of the as-synthesized Ni_2P NCs at different reaction temperature. TEM images illustrate that the as-synthesized Ni_2P NCs exhibit hollow structure and different size distribution. From Fig 4a~f, one can observe that the size of Ni_2P NCs from 65.8 ± 9.9 nm to 95.7 ± 16.9 nm with the increase of temperature from 300 °C to 340 °C, and the Ni_2P NCs exhibit polydispersity, which indicates that the aggregation growth process occurred. The HRTEM image of the Ni_2P NCs with size of 65.8 ± 9.9 nm (Fig. 4g) reveals that the fringe spacing is about 0.221 nm, corresponding to the (111) lattice plane of hexagonal Ni_2P, and the SAED pattern (Fig. 4h) indicates that the as-synthesized Ni_2P NCs have good crystallinity.

The reaction time is another important factor in controlling the size and phase of nickel phosphide NCs. Fig. 5 shows the XRD pattern of the as-synthesized nickel phosphide NCs at different reaction time. It can be seen that all the diffraction peaks match well with the tetragonal structure of $Ni_{12}P_5$ (PDF # 03-065-1623) after the reaction for 10 min. The diffraction peaks at 32.7°, 35.8°, 38.3°, 41.8°, 44.5°, 47.1°, 48.8°, 54.1°, 56.1°, 68.5°, 74.3°, 79.6° and 88.8° are attributed to the (310), (301), (112), (400), (330), (240), (312), (510), (501), (161), (004), (262) and (552) crystal faces, and no extraneous peaks exist, which indicates that the as-synthesized $Ni_{12}P_5$ is a pure phase. The corresponding TEM image (Fig. 6a) exhibits monodisperse tetragonal morphology. The HRTEM image (Fig. 6e) reveals that the fringe spacing is about 0.21 nm, corresponding to the (400) lattice plane of the tetragonal $Ni_{12}P_5$. Furthermore, the SAED pattern (Fig. 6f) also indicates that the as-synthesized $Ni_{12}P_5$ NCs have good crystallinity. However, when the reaction time was prolonged to 60

min, 180 min and 300 min, the crystalline phase was changed. All the diffraction peaks match well with hexagonal structure of Ni_2P, which indicates that increasing the reaction time from 10 min to 5 h leads to a phase transformation from tetragonal $Ni_{12}P_5$ to hexagonal Ni_2P, and we can get conclusion that the shorter reaction time is beneficial for forming $Ni_{12}P_5$ NCs, while the longer reaction time is beneficial for forming Ni_2P NCs. The corresponding TEM images (Fig. 6b~d) further reveal that the size of the as-synthesized nickel phosphide NPs increased and the dispersity became lower. After the reaction time reached 300 min, the dispersity was very poor and most of the particles were aggregate and exhibited polydispersity.

In addition, the effect of OAm quantity on particle size was further investigated. Fig. 7 shows the XRD pattern of the as-synthesized nickel phosphide NCs at different OAm quantity. All the diffraction peaks match well with hexagonal structure of Ni_2P (PDF#03-065-3544), and no extraneous peaks exist. TEM analysis (Fig. 8a~d) indicate that the size of the nickel phosphide NCs changed from 62.5±12.7 to 92.8± 13.9 nm with the quantity of OAm changed from 10 to 15 mL. This is because OAm acts as the reductant to control the nucleation rate, and the presence of excess OAm is in favor of the nucleation process, which leads to the rapid aggregation of the as-synthesized nickel phosphide NCs.

We further studied the electronic properties of the as-synthesized Ni_2P and $Ni_{12}P_5$ NCs. Fig. 9a~b show the XPS spectra in the Ni 2p and P 2p regions of the as-synthesized Ni_2P NCs at 300 °C for 2 h. The peaks at 852.5, 854.8 eV and 860.5 eV can be assigned to Ni in Ni_2P, oxidized Ni species and the satellite of Ni $2p_{3/2}$ peak

for Ni $2p_{3/2}$ energy level, the peaks are observed at 869.5, 873.2 and 877.8 eV can be assigned to Ni in Ni_2P, oxidized Ni species and the satellite of Ni $2p_{1/2}$ peak for the Ni $2p_{1/2}$ energy level, respectively.[11] For the P 2p region, the peaks at 129.5 and 130.1 eV can be assigned to P $2p_{3/2}$ and P $2p_{1/2}$ in Ni_2P, the peak at 133.2 eV can be assigned to small amounts of oxidized P species due to air contact.[22] In addition, the peak at 852.5 eV is positively shifted from that of Ni metal, while the peak at 129.5 eV is negatively shifted from that of elemental P, which indicates that Ni and P have partial positive ($Ni^{\delta+}$, $0<\delta<2$) and negative ($P^{\delta-}$, $0<\delta<1$) charges, respectively. Therefore, we can get a conclusion that there is an electron transfer from Ni to P in Ni_2P NCs. Furthermore, the $Ni_{12}P_5$ NCs have similar Ni 2p and P 2p energy levels as Ni_2P NCs (Fig. 9c~d).

N_2 adsorption-desorption measurements were carried out to further study the textural properties (BET surface area, pore volume, and pore size) of the as-synthesized Ni_2P at 300 °C for 2 h and $Ni_{12}P_5$ NCs at 300 °C for 10 min, as shown in Table 2. The isotherms of the Ni_2P and $Ni_{12}P_5$ NCs are depicted in Fig. 10a. When the relative pressure of Ni_2P NCs reached 0.6, the hysteresis loop appeared. However, no hysteresis loop can be observed in this relative pressure for $Ni_{12}P_5$ NCs. The reason can be attributed to the hollow structure of Ni_2P NCs. The rapid rise of the isotherms indicates the existence of many accumulation pores in Ni_2P and $Ni_{12}P_5$ NCs with the relative pressure exceeded 0.9. The Barrett-Joyner-Halenda (BJH) pore-size distribution curve of Ni_2P NCs (Fig. 10b) shows a narrow peak at 21 nm, and this value is in accord with the size of void observed from TEM (Fig. 4a), indicating that the appearance of this peak is also attributed to the hollow structure of Ni_2P NCs. In

addition, the Ni_2P NCs exhibit a higher BET surface area and pore volume due to the contribution of hollow structure than that of the $Ni_{12}P_5$ NCs.

3.3 Possible growth mechanism

According to the above experimental results, the possible growth mechanism of nickel phosphide NCs could be proposed. The formation process of nickel phosphide NCs consisted of three stages, nucleation, diffusion, aggregation growth process. Previous TG curve (Fig. 2c) indicates that the BTND precursor was decomposed gradually when the temperature reached 200 °C. Meanwhile, OAm acted as solvent, as well as the reductant to form nickel nanoclusters in this temperature.[23] With increasing the reaction temperature to 300 °C, the BTND precursor was decomposed completely and the phosphorization occurred at the same time, the P-C bonds broke and formed the phosphorus atoms, which could diffused into nickel NPs and further formed nickel phosphide NPs. However, the outward diffusion rate of nickel atoms is faster than the inward diffusion rate of phosphorus atoms, which leads to the formation of hollow structure.[10] In addition, the formation of $Ni_{12}P_5$ phase probably due to the phosphorization process was not completed at short reaction time, and the increase of the reaction time is favorable to the phosphorization process. The small size NPs were unstable in solution due to the high surface energy and intermolecular forces,[23] and the particles aggregation process increased correspondingly, which leads to the formation of Ni_2P NPs with broad size distribution and low dispersity.

4. Conclusions

An effective one-pot thermal decomposition method was described to synthesize

nickel phosphide NCs using bis(triphenylphosphine)nickel dichloride as the single-source precursor in presence of OAm. This method also could be used to synthesize others transition metal phosphides. The size of the Ni_2P NCs can be controlled by changing reaction temperature and OAm quantity. The phase of the nickel phosphide NCs can be controlled by changing reaction time. Generally, shorter reaction time was beneficial for forming $Ni_{12}P_5$ NCs, and longer reaction time was beneficial for forming Ni_2P NCs. The formation mechanism of nickel phosphide NCs consisted of three stages: nucleation, diffusion and aggregation growth process. In short, this paper offers a simple method of creating a variety of transition metal phosphides with controllable size and phase.

Acknowledgements

This work was financially supported by the National Natural Science Foundation of China (Grants No. 21006128, 21176258, U1162203), China University of Petroleum for Postgraduate Technology Innovation Project (Grants No. YCX2014033) and the Specialized Research Fund for the Doctoral Program of Higher Education of China (Grant No. 20110133110002).

References

1 K. Y. Yoon, Y. J. Jang, J. Park, Y. Hwang, B. Koo, J. G. Park and T. Hyeon, *J. Solid State Chem.*, 2008, **181**, 1609.

2 C. Qian, F. Kim, L. Ma, F. Tsui, P. D. Yang and J. Liu, *J. Am. Chem. Soc.*, 2004, **126**, 1195.

3 X. C. Jiang, Q. H. Xiong, S. Nam, F. Qian, Y. Li and C. M. Lieber, *Nano Lett.*, 2007,

7, 3214.

4 L. M. Song and S. J. Zhang, *Powder Technol.*, 2011, **208**, 713.

5 L. M. Song, S. J. Zhang and Q. W. Wei, *Catal. Commun.*, 2011, **12**, 1157.

6 Y. H. Ni, K. M. Liao and J. Li, *CrystEngComm*, 2010, **12**, 1568.

7 E. J. Popczun, J. R. McKone, C. G. Read, A. J. Biacchi, A. M. Wiltrout, N. S. Lewis and R. E. Schaak, *J. Am. Chem. Soc.*, 2013, **135**, 9267.

8 K. Mi, Y. H. Ni and J. M. Hong. *J. Phys. Chem. Solids*, 2011, **72**, 1452.

9 J. Park, B. Koo, K. Y. Yoon, Y. Hwang, M. Kang, J. G. Park and T. Hyeon, *J. Am. Chem. Soc.*, 2005, **127**, 8433.

10 R. K. Chiang and R. T. Chiang, *Inorg. Chem.*, 2007, **46**, 369.

11 Y. Z. Chen, H. D. She, X. H. Luo, G. H. Yue and D. L. Peng, *J. Cryst. Growth*, 2009, **311**, 1229.

12 X. F. Qian , X. M. Zhang, C. Wang, W. Z. Wang and Y. T. Qian, *Mater. Res. Bull*, 1998, **33**, 669.

13 H. L. Su, Y. Xie, B. Li, X. M. Liu, and Y. T. Qian, *Solid State Ionics*, 1999, **122**, 157.

14 S. L. Liu, X. Z. Liu, L. Q. Xu, Y. T. Qian and X. C. Ma, *J. Cryst. Growth*, 2007, **304**, 430.

15 G. Berhault, P. Afanasiev, H. Loboué, C. Geantet, T. Cseri, C. Pichon, C. Guillot-Deudon and A. Lafond, *Inorg. Chem.*, 2009, **48**, 2985.

16 G. J. Shi and J. Y. Shen, *J. Mater. Chem.*, 2009, **19,** 2295.

17 X. L. Hu and J. C. Yu, *Chem. Mater.*, 2008, **20**, 6743.

18 E. Muthuswamy, G. H. Layan Savithra and S. L. Brock, *ACS Nano*, 2011, 5, 2402.

19 B. Singh, C. L. Ho, Y. C. Tseng and C. T. Lo, *J. Nanopart. Res.*, 2012, **14**, 706.

20 X. F. Zheng, S. L. Yuan, Z. M. Tian, S. Y. Yin, J. H. He, K. L. Liu and L. Liu, *Mater. Lett*, 2009, **63**, 2283.

21 E. Standley, S. J. Smith, P. Müller and T. F. Jamison, *Organometallics*, 2014, **33**, 2012.

22 D. Q. Zhang, G. S. Li and J. C. Yu, *Cryst. Growth & Des.*, 2009, 9, 2812.

23 Y. Pan, R. R. Jia, J. C. Zhao, J. L. Liang, Y. Q. Liu and C. G. Liu, *Appl. Surf. Sci*, 2014, **316**, 276.

Figure Captions

Fig. 1 Synthetic route of Ni_2P NCs.

Fig. 2 FTIR spectrum (a), ^{13}C NMR spectrum (b) and TG-DSC curve (c) of the BTND precursor.

Fig. 3 XRD pattern of the as-synthesized nickel phosphide NCs at different reaction temperature.

Fig. 4 TEM images and size distributions of the as-synthesized Ni_2P NCs at different reaction temperature of (a, b) T = 300 ℃; (c, d) T = 320 ℃; (e, f) T = 340 ℃; HRTEM image (g) and SAED pattern (h) of Ni_2P NCs at 300 ℃ for 2 h.

Fig. 5 XRD pattern of as-synthesized nickel phosphide NCs at different reaction time.

Fig. 6 TEM images of the as-synthesized nickel phosphide NCs at different time of (a) t= 10 min; (b) t= 60 min; (c) t= 180 min; (d) t= 300 min. HRTEM image (e) and SAED pattern (f) of $Ni_{12}P_5$ NCs at 300 ℃ for 10 min.

Fig. 7 XRD pattern of the as-synthesized nickel phosphide NCs at different OAm quantity.

Fig. 8 TEM images and size distributions of the as-synthesized Ni_2P NCs at different OAm quantity of (a, b) OAm = 10 mL; (c, d) OAm = 15 mL.

Fig. 9 XPS spectra of the Ni 2p and P 2p regions for (a, b) Ni_2P at 300 ℃ for 2 h and (c, d) $Ni_{12}P_5$ NCs at 300 ℃ for 10 min.

Fig. 10 N_2 adsorption-desorption isotherms (a) and BJH pore-size distribution (b) of as-synthesized Ni_2P at 300 ℃ for 2 h and $Ni_{12}P_5$ NCs at 300 ℃ for 10 min.

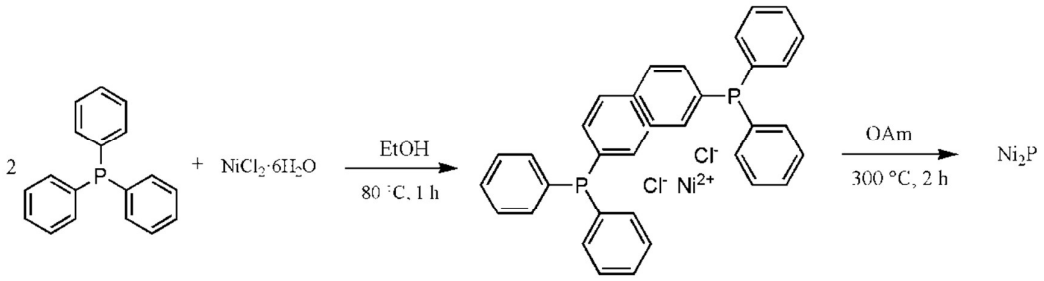

Fig. 1 Synthetic route of Ni_2P NCs

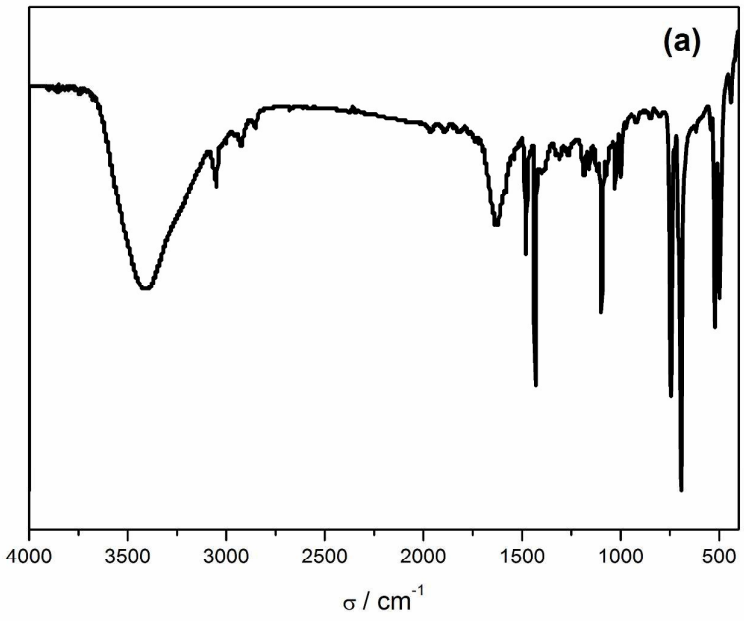

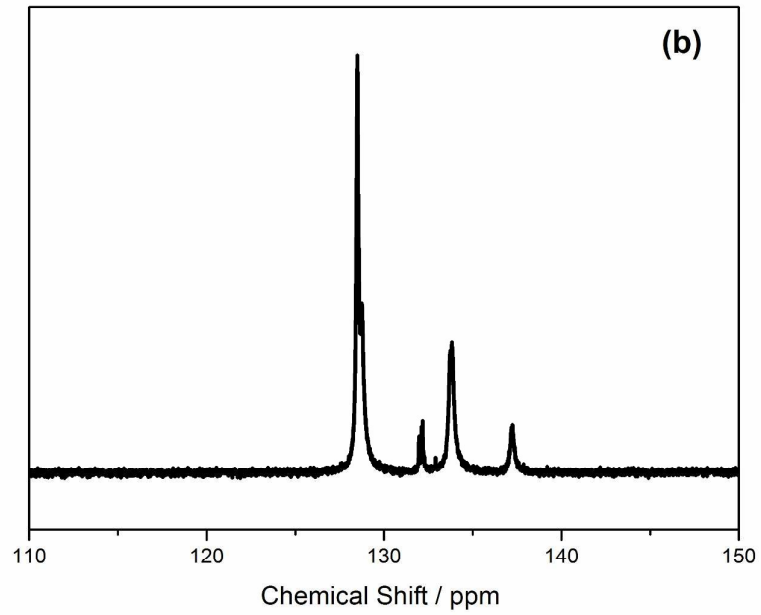

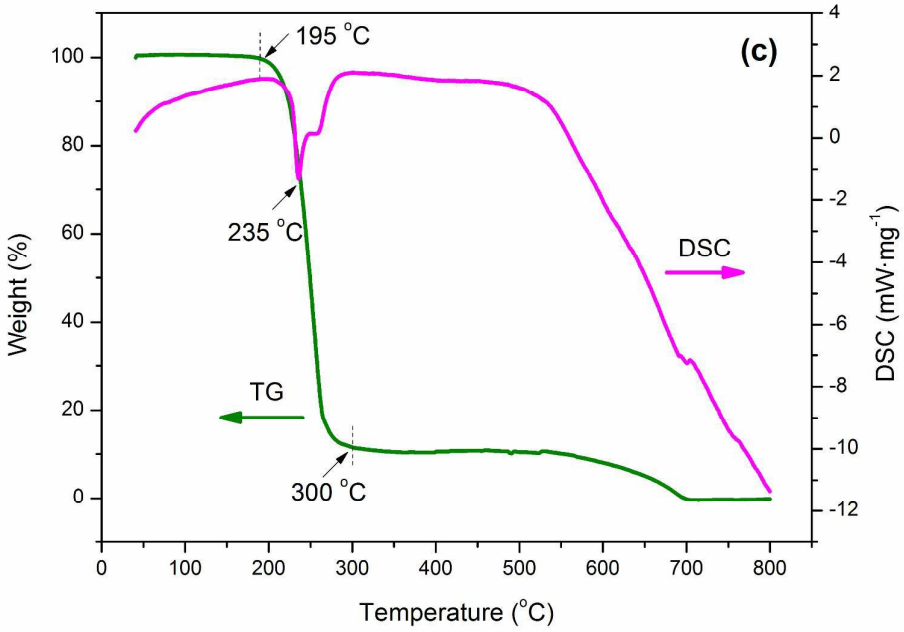

Fig. 2 FTIR spectrum (a), ^{13}C NMR spectrum (b) and TG-DSC curve (c) of the BTND precursor.

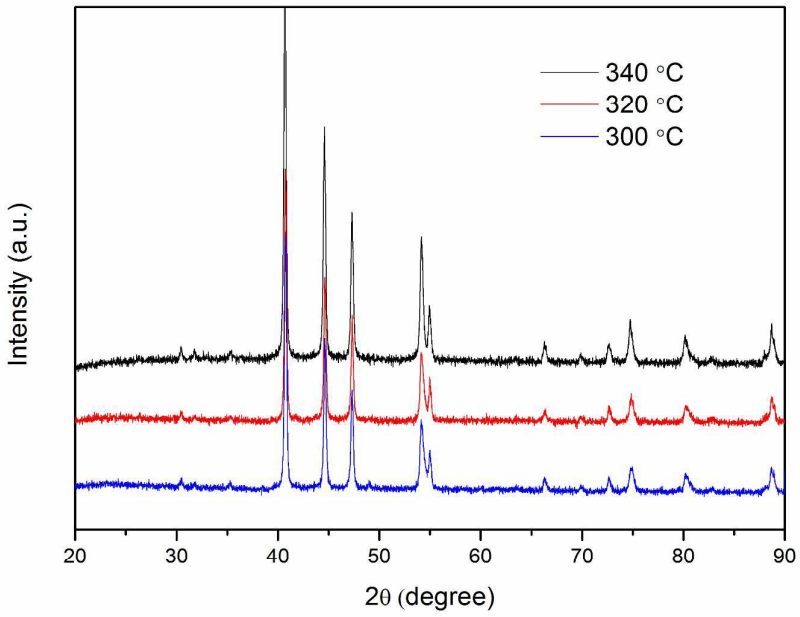

Fig. 3 XRD pattern of the as-synthesized nickel phosphide NCs at different reaction temperature.

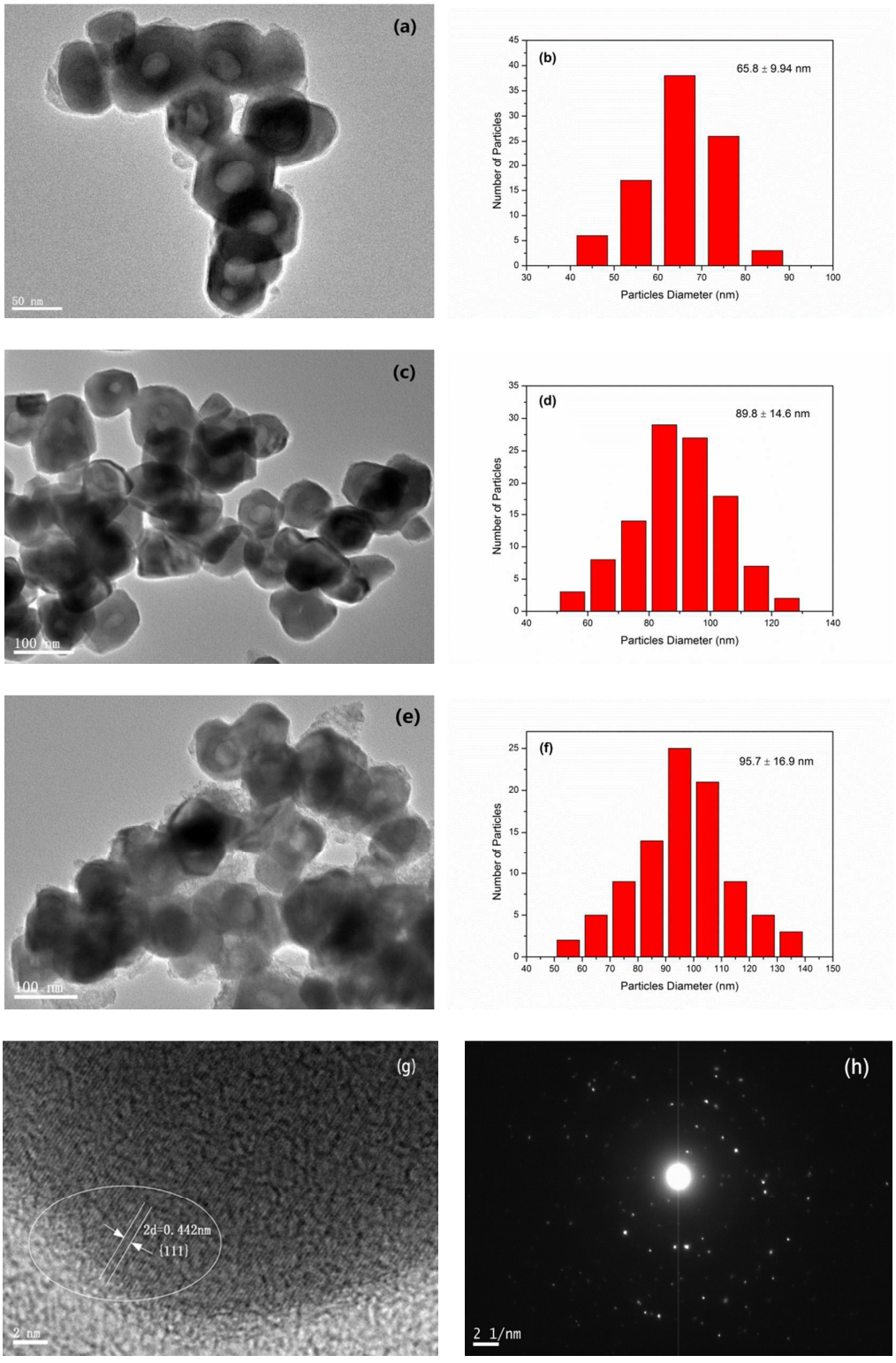

Fig. 4 TEM images and size distributions of the as-synthesized Ni_2P NCs at different reaction temperature of (a, b) T = 300 °C; (c, d) T = 320 °C; (e, f) T = 340 °C;

HRTEM image (g) and SAED pattern (h) of Ni_2P NCs at 300 ℃ for 2 h.

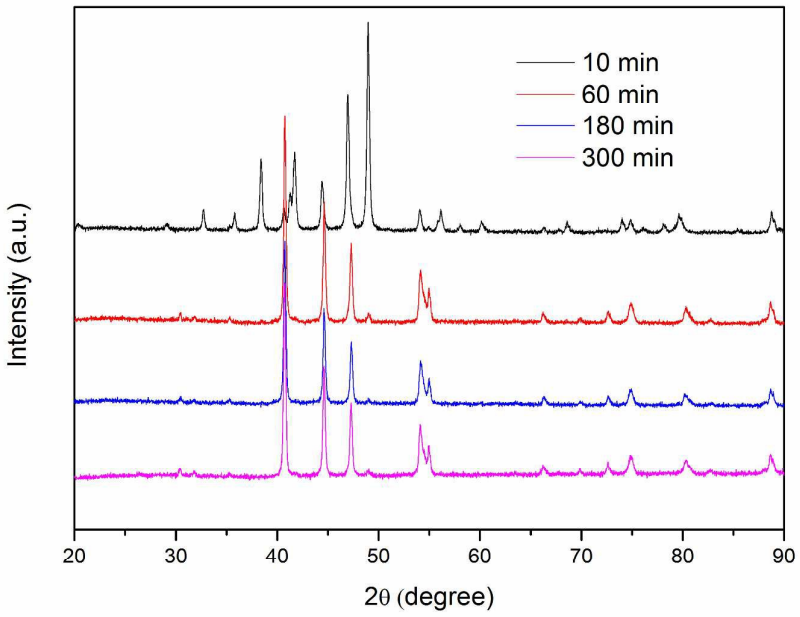

Fig. 5 XRD pattern of as-synthesized nickel phosphide NCs at different reaction time.

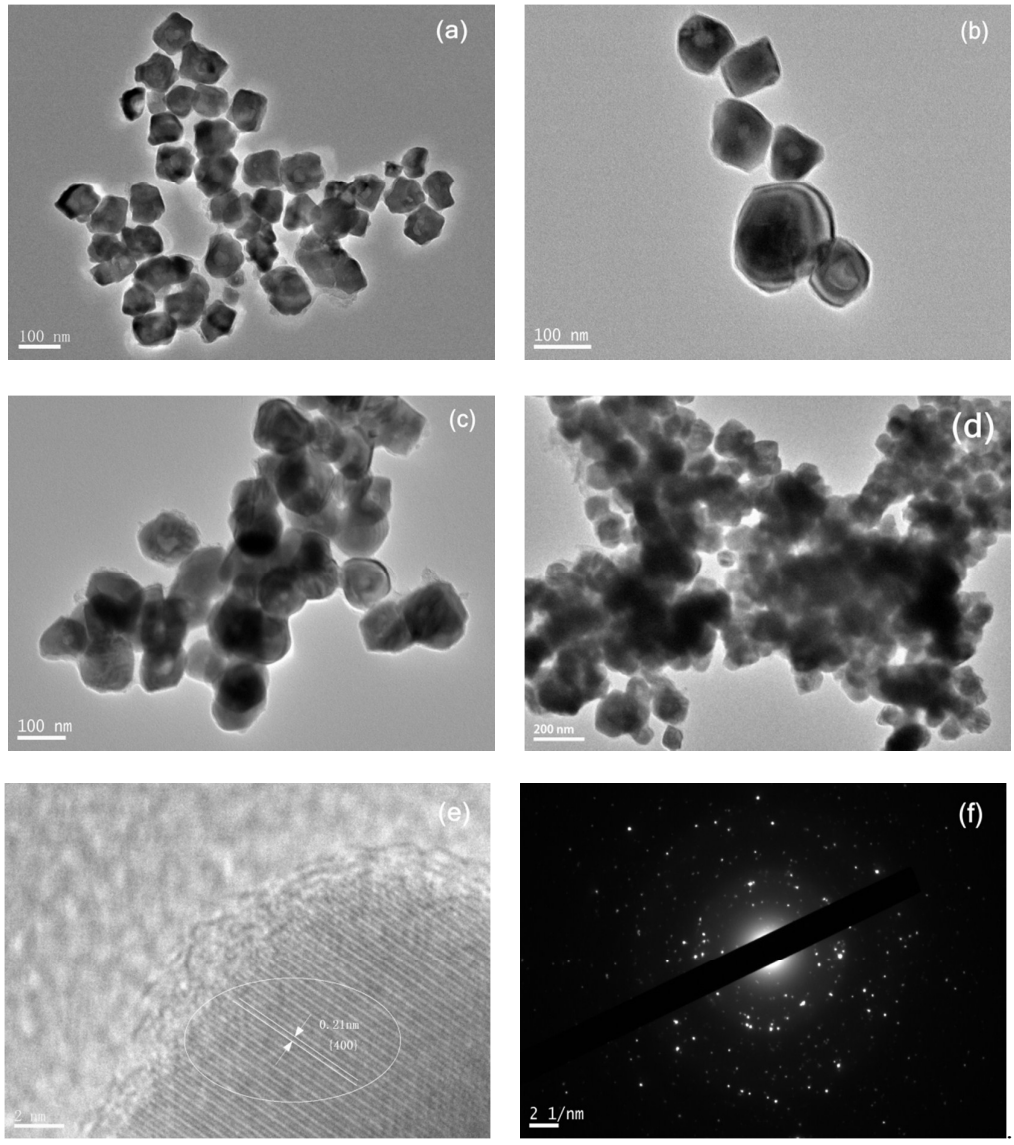

Fig. 6 TEM images of the as-synthesized nickel phosphide NCs at different time of (a) t= 10 min; (b) t= 60 min; (c) t= 180 min; (d) t= 300 min. HRTEM image (e) and SAED pattern (f) of $Ni_{12}P_5$ NCs at 300 °C for 10 min.

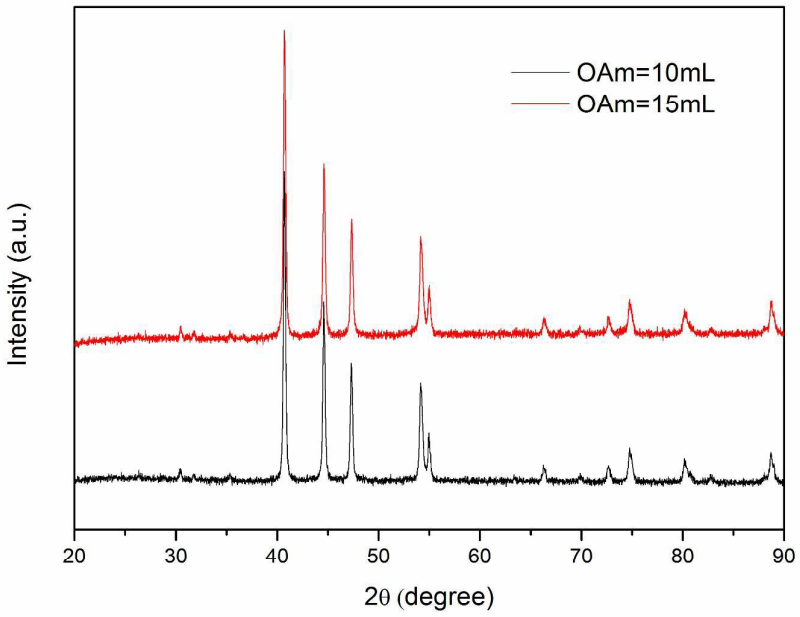

Fig. 7 XRD pattern of the as-synthesized nickel phosphide NCs at different OAm quantity.

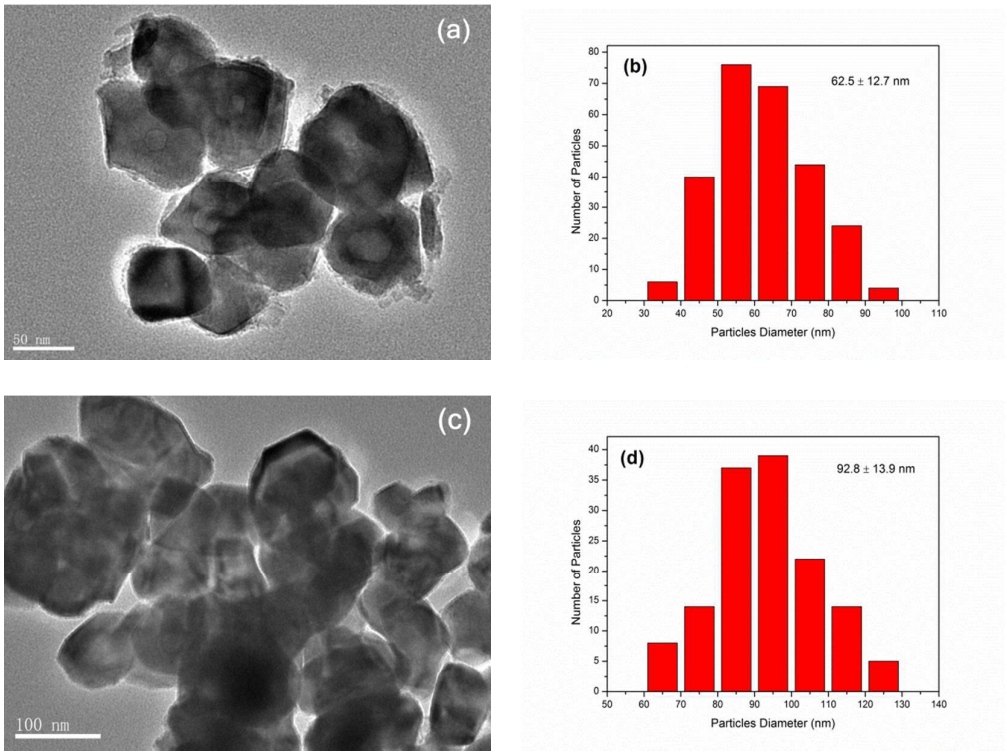

Fig. 8 TEM images and size distributions of the as-synthesized Ni_2P NCs at different OAm quantity of (a, b) OAm = 10 mL; (c, d) OAm = 15 mL.

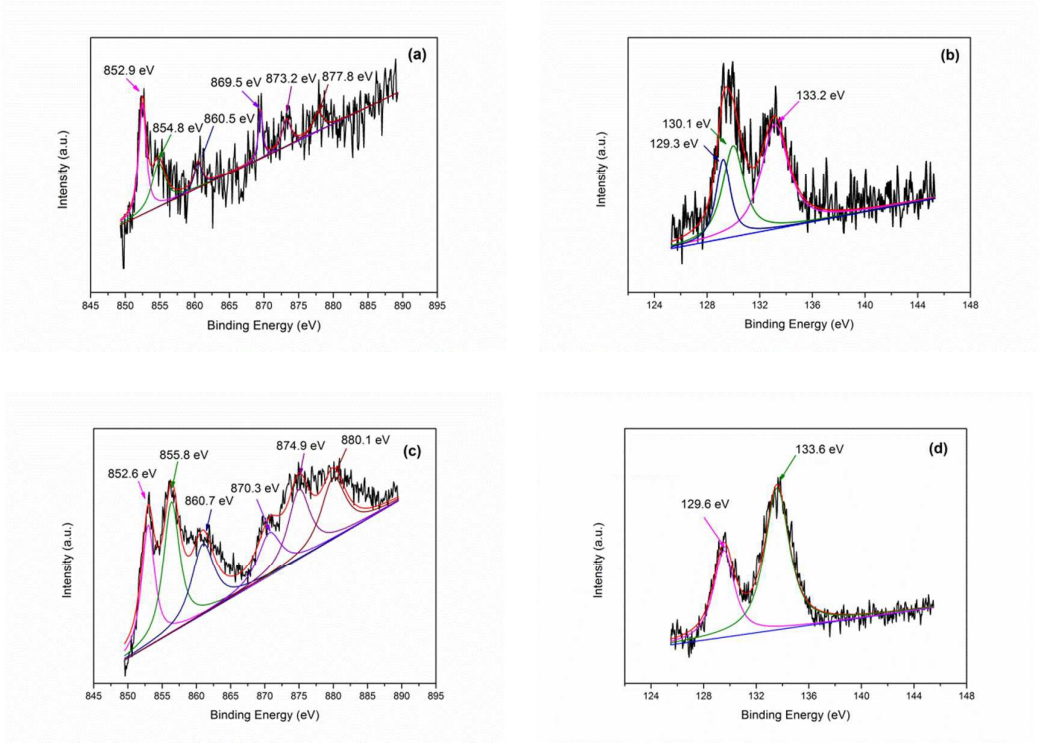

Fig. 9 XPS spectra of the Ni 2p and P 2p regions for (a, b) Ni_2P at 300 °C for 2 h and (c, d) $Ni_{12}P_5$ NCs at 300 °C for 10 min.

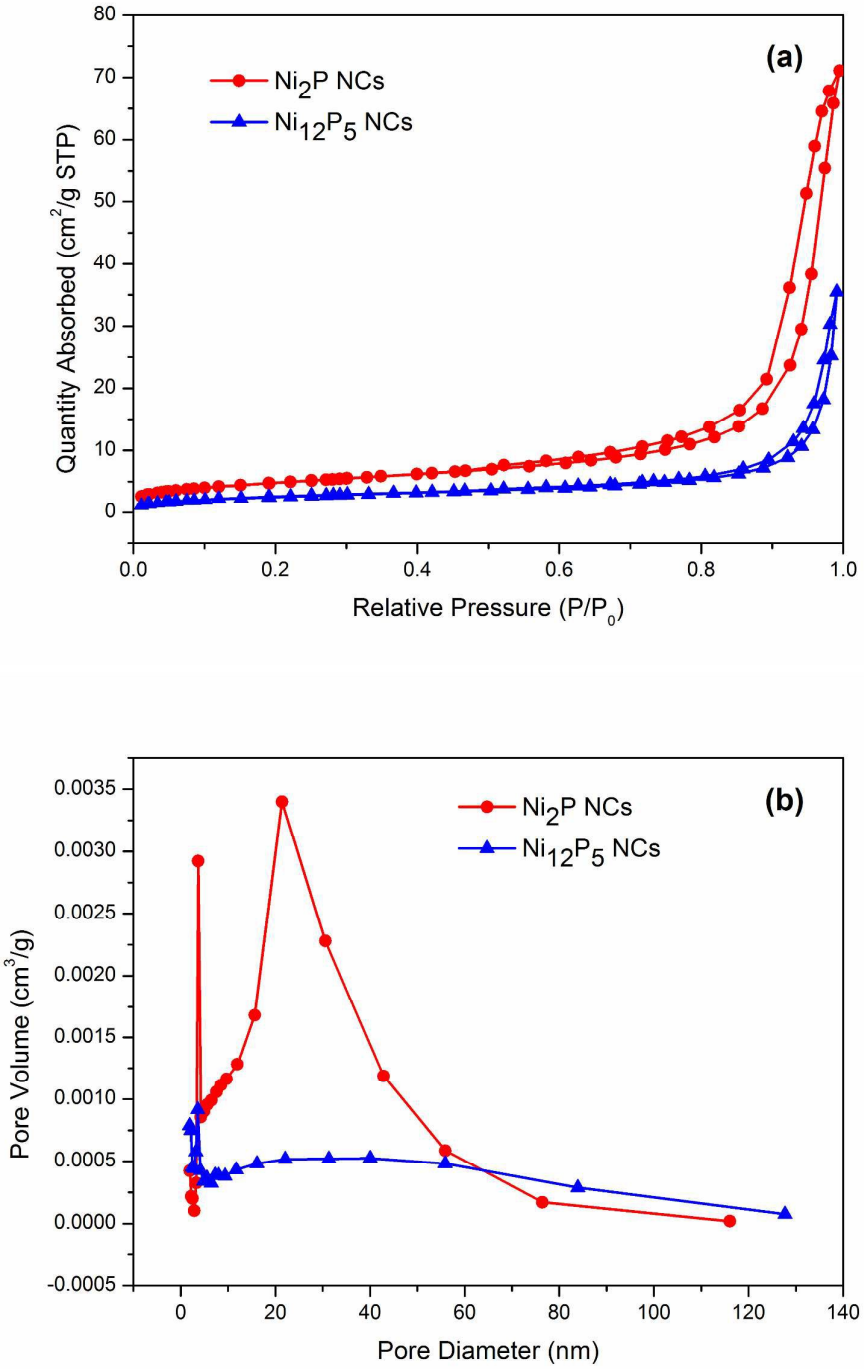

Fig. 10 N_2 adsorption-desorption isotherms (a) and BJH pore-size distribution (b) of as-synthesized Ni_2P at 300 ℃ for 2 h and $Ni_{12}P_5$ NCs at 300 ℃ for 10 min.

Table 1 Detailed synthetic conditions of the single-factor experiment.

Group	T (°C)	T (min)	OAm (mL)	Product
	300	120	5	Ni_2P
a	320	120	5	Ni_2P
	340	120	5	Ni_2P
	300	10	5	$Ni_{12}P_5$
b	300	60	5	Ni_2P
	300	180	5	Ni_2P
	300	300	5	Ni_2P
c	300	120	10	Ni_2P
	300	120	15	Ni_2P

Table 2 Textural properties of the as-synthesized Ni_2P NCs at 300 °C for 2 h and $Ni_{12}P_5$ NCs at 300 °C for 10 min.

	BET surface area (m^2/g)	Pore volume (cm^3/g)	Pore size (nm)
Ni_2P	17.3	0.1	21.1
$Ni_{12}P_5$	9.3	0.05	25.5

Highlights

- We report an efficient method for the synthesis of nickel phosphide NCs for the first time.
- A possible growth mechanism of nickel phosphide NCs is proposed.
- The size of Ni_2P NCs can be controlled by changing reaction temperature and OAm quantity.
- The phase of nickel phosphide NCs can be controlled by increasing reaction time.
- These synthetic techniques may be expanded to other metal phosphide materials.